AIChE

Axial Segregation in Bubbling Gas-Fluidized Beds with Gaussian and Lognormal Distributions of Geldart Group B Particles

Jia Wei Chew, Jeffrey R. Wolz, and Christine M. Hrenya
Dept. of Chemical and Biological Engineering, University of Colorado at Boulder, Boulder, CO 80309

DOI 10.1002/aic.12219
Published online April 22, 2010 in Wiley Online Library (wileyonlinelibrary.com).

Bubbling, gas-fluidized bed experiments involving Geldart Group B particles with continuous-size distributions have been carried out. Sand of various widths of Gaussian or lognormal distributions were completely fluidized, then axial concentration profiles were obtained from frozen-bed sectioning. Similar to previous works on binary systems, results show that mean particle diameter decreases with increasing bed height, and that wider Gaussian distributions show increased segregation extents. Surprisingly, however, lognormal distributions exhibit a nonmonotonic segregation trend with respect to distribution widths. In addition, the shape of the local-size distribution is largely preserved with respect to that of the overall distribution. These findings on the nature of local-size distribution provide experimental confirmation of previous results for granular and gas-solid simulations. Lastly, an interesting observation is that although monodisperse Geldart Group D particles cannot be completely fluidized, their presence in lognormal distributions investigated still results in complete fluidization of all particles. *AIChE J,* 56: 3049–3061, 2010
Keywords: bubbling gas-fluidized bed, continuous particle size distribution (Gaussian, lognormal), segregation, polydisperse, fluidization

Introduction

Flows involving solid particles are used extensively in industry (energy production, materials synthesis, pollution control, pharmaceuticals, etc.), and are also found in natural environments (landslides, avalanches, planetary rings, etc.). A historically important unit operation that utilizes such flows is the fluidized bed. The first industrial-scale, commercially-significant use of the fluidized bed was Winkler's coal gasifier, which commenced operation in 1926.[1] Fluidization then progressed to hit the industrial scene in a widespread way in 1942 with catalytic cracking.[1] Fluidized beds have several unique qualities which make them desirable for industrial operations, including high heat and mass transfer between gas and particles, suitability for large-scale operations, ease of operation due to the liquid-like flow of particles, and so on.[1–3] However, since the fundamental flow behavior of such systems is still not well understood, the prediction, design and operation of related systems are often based on experience rather than on scientific principles. As a result, processes employing particulate flows often operate below design capacity and exhibit undesirable flow behavior.[4,5]

Gas-solid interaction is crucial to reactor performance. Because the particles in bubbling fluidized beds are often not monodisperse, the different particle sizes de-mix, or segregate, according to species.[6–8] Hence, an enhanced understanding of polydisperse flows will allow for an improvement of such existing operations and a more efficient design of new operations. Yet, despite the prevalence of *continuous*-size distributions in industrial fluidized beds, most

Correspondence concerning this article should be addressed to C. M. Hrenya at hrenya@colorado.edu.

previous segregation studies have been focused on *binary* mixtures consisting of two particle types of different sizes and/or densities. A brief review of species segregation experiments and simulations in fluidized beds with binary mixtures has been presented by Joseph et al.[9] Comparatively, few efforts have been devoted to the investigation of continuous-size distributions; these previous contributions are described next.

Experimental results have been presented on the impact of continuous-size distributions on the fluid mechanical behavior of bubbling beds, with effects ranging from minimum fluidization velocity,[10–12] bubble sizes,[13] pressure fluctuations,[14] presence of particles in bubbles,[10,15] etc. The contribution by Grace and Sun[14] represents one of the earliest reviews on the influence of particle-size distribution (PSD) on the quality of fluidization, and they summarized that a wider PSD (of Geldart Group A particles) culminates in enhanced reactor efficiency through improved interphase mass transfer and better gas-solid contacting. One factor impacting gas-solid interaction is the degree of species segregation, and a few efforts have reported on species segregation for continuous size distributions.[11,16,17] Hoffman and Romp[16] investigated a Gaussian distribution of Group B particles with a distribution width of 30% (i.e., ratio of standard deviation, σ, to the mass-averaged diameter, d_{ave}), under various superficial velocities (U_s). They found segregation of the smallest and largest particles, respectively, at the upper and lower layers of the bed, which is qualitatively similar to previous findings for binary mixtures.[9,18–20] Because of the presence of more size species, concentration maxima of particles of different sizes at different heights were observed along the bed. It was also found that species segregation continues to exist for velocities significantly higher than the minimum fluidization velocity. This particular Gaussian distribution reported is also one of the distributions investigated in this work. Lin and Wey[17] and Gauthier et al.[11] both compared a narrow cut, a binary mixture, a uniform distribution and a Gaussian distribution to examine how different PSD's affect fluidization. Lin and Wey[17] found that the narrow cut and Gaussian distribution exhibited the best fluidization quality, which was defined as the least amount of pressure fluctuations. Gauthier et al.[11] further observed that Gaussian PSD and narrow cut hardly segregate, whereas binary and flat PSD mixtures always segregate. Collectively, these experimental works provide some insight on how continuous distributions segregate relative to other types of distributions. What is still missing is the impact of the width of continuous distributions on segregation behavior, which is addressed in this work.

In addition to the experimental works on continuous PSD's in bubbling beds discussed previouslly, a number of modeling efforts supplement the experimental results. Size-segregation in gas-solid fluidized beds containing continuous PSD's has been examined via Eulerian-Lagrangian[21] and Eulerian-Eulerian[22] simulations, with both indicating that wider distributions show more extensive segregation than narrower ones. Earlier molecular-dynamics (or equivalently, discrete element modeling (DEM)) simulations involving granular flow (i.e., no interstitial fluid) led to a similar conclusion.[23] More specifically, Dahl and Hrenya[21] employed an Eulerian-Lagrangian model of a gas-solid fluidized bed to investigate the species segregation (de-mixing) behavior of both Gaussian and lognormal distributions over a range of distribution widths, restitution and friction coefficients, and gas velocities. The results indicate that: (1) the average particle diameter decreases as the height within the bed increases, (2) the level of segregation increases with an increase in the width of the PSD, and (3) shape of the local-size distribution (i.e., Gaussian or lognormal) is found to mimic that of the overall size distribution in most regions of the fluidized bed. To date, experimental validation of points (2) and (3) have not been pursued, this serves as further motivation of this work. Due to the assumptions incorporated in such simulations, experimental validation of models is important. In particular, recent work has indicated that the drag-law treatment plays a crucial role in the qualitative and quantitative nature of segregation of polydisperse systems.[24,25] In the earlier DEM simulations of Dahl and Hrenya,[21] however, an *ad hoc* treatment of the polydisperse drag law was used since more rigorous, lattice-Boltzmann-based treatments[26,27] were not yet available.

In an effort to build on the previous knowledge on the effect of continuous-size distributions on species segregation, the objective of the current work is twofold: (1) to experimentally determine the impact of the width of the distribution on the degree of segregation, and (2) to experimentally determine the shape of local-size distributions throughout the bed. Experiments have been carried out involving both Gaussian and lognormal PSD's of Geldart Group B particles in low-velocity bubbling beds, with an emphasis on axial concentration profiles. The results validate the trends observed in previous simulations[21] in terms of the segregation of larger particles to the bottom of the bed, a positive correlation between width of Gaussian distribution and segregation extent, and a general preservation of the shapes of local distributions. A surprising fourth finding, however, lies in the nonmonotonic behavior of segregation extents with widths of lognormal distributions. Specifically, as the width of a lognormal distribution increases, the segregation extent increases and then decreases.

Finally, although not a primary focus of the current effort, interesting observations were also made for the fluidization behavior of Geldart Group D particles. Albeit the focus of this work being on Geldart group B particles, it is important to note that wide PSD's may, by necessity, span more than one Geldart group. This work presents evidence that the presence of Group B and D particles in a continuous distribution allow the Group D particles constituents to be fully fluidized even when a monodisperse suspension of the same Group D particles do not completely fluidize. The poor fluidization quality of the Group D particles is evidenced by the discrepancy between the actual bed mass and that calculated via the fluidization curve data.

Experimental Description

Fluidized-bed setup

A schematic diagram of the experimental setup for all fluidization experiments is shown in Figure 1, which is identical to that used by Joseph et al.[9] Particles are fluidized in a Plexiglas column which is 18.5 cm in diameter. A Yaskawa V7 variable frequency drive controls a Fuji Electric VFD5

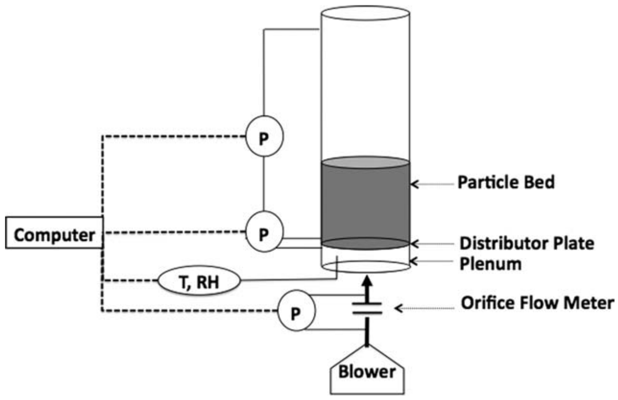

Figure 1. Schematic of fluidized-bed experimental setup.

regenerative blower that provides the air for fluidization. A National Instruments LabVIEW program (version 7.1) remotely controls the driver. A Mott Corp. 316 stainless steel sintered porous plate, with an average porosity of 40% and 1.6 mm thickness, serves as the distributor plate. The superficial velocity (U_s), which is reported at local atmospheric conditions (air with a 0.97 kg/m^3 density and 1.85 $\times$ 10^{-5} Pa·s viscosity), is determined based on measurements via a Lambda Square Oripac 4150-P orifice plate flow meter, which is located upstream of the plenum. Relative humidity (RH) in the unit is enhanced by an Air-O-Swiss model AOS 7144 humidifier placed at the inlet of the blower. Relative humidity (RH) is kept above 40% for all experiments to help reduce electrostatics.[28–31] The operating air temperature and RH in the plenum are measured by means of an Omega HX93AV-RP1 probe, with a temperature range of −4–171°C, and RH range of 0–100%, inserted into the plenum. The pressure drops across the orifice plate flow meter, across the distributor plate, and across the entire fluidized bed are measured using Orange Research 20100 Series low-differential pressure transmitters with the ±0.2% accuracy option. Pressure drop statistics across the orifice meters are transmitted to the computer and superficial velocities computed. For all experiments, pressure drop across the distributor was always at least 100% that across the fluidized bed, hence, ensuring uniform distribution of air upward into the column. All temperature, relative humidity, superficial velocity and pressure data are recorded throughout the experiments.

Particle-Size Distributions

Two continuous-size distributions, namely Gaussian and lognormal, were examined using sand particles. The sand was acquired from US Silica Co., with a specific gravity of 2.65. Various distribution widths were examined; the distribution width is defined as the ratio of standard deviation (σ) of particle size to Sauter-mean diameter (d_{sm}). The range of σ/d_{sm} used for Gaussian distributions is 10 to 30%. These lower and upper limits are specified such that the system will not resemble a monodisperse system, and will not require negatively-sized particles, respectively. The range of σ/d_{sm} used for lognormal distributions is 10 to 70%. The lower limit is 10% because it is observed that a lognormal distribution with σ/d_{sm} = 10% is similar to the Gaussian distribution with the same σ/d_{sm}, so the results for the Gaussian distribution with σ/d_{sm} = 10% will be used in the analysis for lognormal distributions too. The upper limit is established to avoid using sand particles of greater than 2.8 mm, which are scarce.

As mentioned previously, this effort focuses on Geldart Group B particles fluidized by air under atmospheric conditions. For operation strictly within Geldart Group B classification,[32] the size range of the sand particles was calculated to be 80–670 μm, and this is the range used for all Gaussian distributions investigated. For the wider lognormal distributions (σ/d_{sm} > 30%); however, some bigger particles in the Geldart Group D classification were required since the entire Geldart Group B range was not wide enough to contain the full distribution of particle sizes. The Sauter-mean diameter (d_{sm}) of all the Gaussian and lognormal distributions under investigation was set to 375 μm, which is the middle value of the stipulated Group B size range. The size distributions used in the experiments were prepared based on exact expressions for the mass-based frequency distribution function (f_m) for Gaussian and lognormal systems

$$f_{m,\text{Gaussian}} = \frac{1}{\sigma\sqrt{2\pi}}\exp\left[-\frac{(x-d_{sm})^2}{2\sigma^2}\right] \tag{1}$$

$$f_{m,\text{lognormal}} = \frac{1}{x\sigma\sqrt{2\pi}}\exp\left[-\frac{(\ln(x)-d_{sm})^2}{2\sigma^2}\right] \tag{2}$$

where x is the particle size. Shown in Figure 2 are the Gaussian (Figure 2a), and lognormal (Figure 2b) distributions (f_m), obtained, respectively by Eqs. 1 and 2 and denoted by lines, as well as the experimental values obtained via sieving and denoted by points. More specifically, the experimental value of f_m is determined as the ratio of the mass fraction to width of the particle-size bin (as determined by the sieve cutoffs); note the division by bin width serves as a normalization to provide a straightforward means of comparison between bins of different widths.[33] Fisherbrand U.S. Standard Brass Test Sieves, 0.203 m dia. $\times$ 0.051 m height, were used for preparing the particle-size distributions (PSD). Figure 2 illustrates the close correspondence between the exact and experimental distributions. Notably, the particle sizes for all widths of Gaussian distributions investigated are contained in the Geldart Group B classification (80–670 μm), while up to 24% by mass of the widest lognormal distribution (σ/d_{sm} = 70%) falls in the Geldart Group D classification. As mentioned previously, due to the nature of the lognormal distribution, it is not possible to restrict all particle sizes to within Group B classification, and larger Group D particles have to be included for an accurate representation.

Prior to any size classification, sand acquired from the vendor was fluidized at greater than three times the complete fluidization velocities (U_{cf}, as later detailed) for at least 100 h. The high-velocity fluidization was necessary to smooth out the rough edges of the particles to avoid further attrition so as to preserve the integrity of PSD's during fluidization experiments. Validation tests have also been carried out to ensure reproducibility and reliability of the sieving technique used for measuring PSD's. In particular, care was taken to ensure each sieve tray was never more than half full, and an

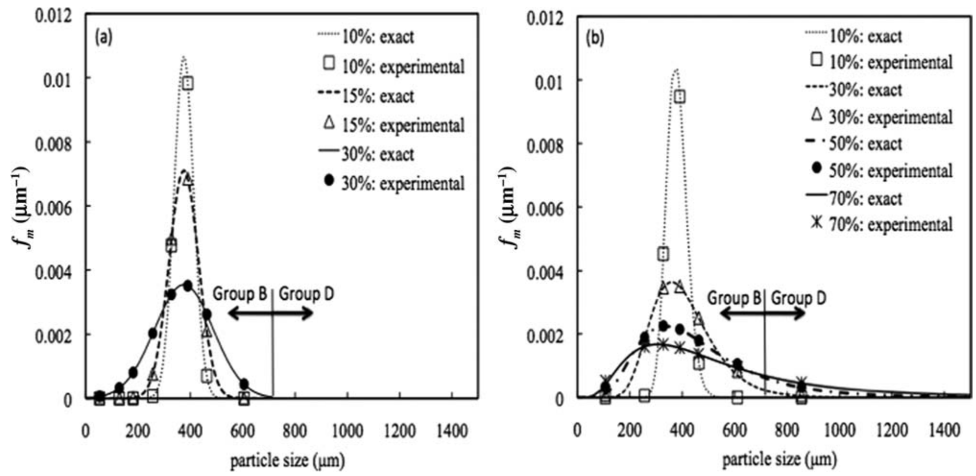

Figure 2. Frequency distributions of (a) Gaussian with σ/d_{sm} = 10, 15, and 30%, and (b) lognormal with σ/d_{sm} = 10, 30, 50, and 70%.

The lines represent exact distributions as defined by Eqs. 1 and 2, while the discrete points are experimental values.

adequate sieve-shaking duration was observed depending on the loading size. For example, for a 2 kg sample, a sieve-shaking duration of 10 min and more gave the same sieve results; hence, sieve duration of 10 min was determined to be sufficient.

Axial Concentration Measurements

As a precursor to the axial concentration (or segregation) measurements, fluidization curves were first generated to determine U_{cf}, the *complete* fluidization (superficial) velocity, which is defined as the velocity beyond which the pressure drop across the bed remains constant. To determine U_{cf}, the particle bed of a given distribution underwent repeated cycles of defluidization-fluidization over a range of superficial velocities (U_s) to generate the fluidization curves, which are plots of pressure drop (ΔP) vs. U_s. Defluidization was always run first to ensure a repeatable initial state for subsequent fluidization, and three cycles of defluidization-fluidization were carried out for each distribution. Superficial velocities (U_s) were decreased or increased incrementally by 0.01 m/s, and held at each step for 40 s, after which pressure drop across the bed is averaged over 10 s. For all the distributions investigated, the pressure drop at which the curve plateaus for higher U_s (i.e., $U_s > U_{cf}$) is equal to the ratio of the bed weight over cross-sectional area (W/A), which provides evidence of complete fluidization. Due to some noise present in the data, a systematic method of U_{cf} determination was employed, namely defining U_{cf} as the average U_s of the first 5% of the total number of points that fall within ± 1% of the expected W/A value.

To ensure repeatable initial conditions for the segregation experiments,[9] the bed was initially mixed at a high-superficial velocity, specifically $U_s = 3U_{cf}$, before lowering it to the desired value of $1.2U_{cf}$ used in the segregation experiments. An adequate duration for this initial mixing was carefully determined, and after fluidizing the bed for a stipulated duration, the PSD from an axial section at a dimensionless height (H^*) of 0.5 was measured via sieving. H^* is defined as the height of the axial section normalized with the collapsed bed height. Because the Gaussian distribution with $\sigma/d_{sm} = 30\%$ was found to display among the most significant segregation (described later), it was used for this portion of the investigation. At $3U_{cf}$, essentially superimposable PSD's were observed for durations ranging from 15 min to 1 h, implying that 15 min is sufficient to generate reproducible initial conditions. Hence, the bed was allowed to initially mix at $3U_{cf}$ for 15 min before the velocity was lowered for the subsequent segregation experiments. The same procedure was used in the investigation of binary mixtures by Joseph et al.[9]

After the initial mixing period described previously, the gas velocity was adjusted to the lower value, namely $1.2U_{cf}$, for which steady-state axial concentration profiles are obtained. The value of $1.2U_{cf}$ was chosen because the operating U_s has to be high enough to ensure that the bed is thoroughly fluidized, and yet low enough such that subsequent bed freezing does not lead to further segregation during bed collapse. The duration required to achieve steady-state and reproducibility was also investigated. The Gaussian distribution with $\sigma/d_{sm} = 30\%$ was used again for the same reason described previously. The bed was fluidized at $1.2U_{cf}$ for various durations (namely, 30 min, 1 h, 2 h, and 60 h). While segregation was incomplete at 30 min, the system appeared to have reached steady state at 1 h and beyond. Hence, the air supply was quickly shut off and the plenum vented to freeze the bed after 1 h of fluidization at $1.2U_{cf}$. Axial concentration profiles were then measured by vacuuming out axial sections of the collapsed bed and sieving the resulting samples. Radial segregation was found to be insignificant relative to variations in the axial direction, and, hence, only axial concentration profiles are reported.[9]

In summary, the procedure for the segregation experiments is as follows: (1) Load 8 kg of sand with the stipulated distribution into the column; (2) generate a defluidization-fluidization curve in order to determine U_{cf}; (3) mix the bed for 15 min at high velocity ($3U_{cf}$) to generate reproducible initial conditions for the subsequent low-velocity fluidization; (4) fluidize the bed at low velocity ($1.2U_{cf}$) for a period sufficient (1 h) for steady-state segregation to be

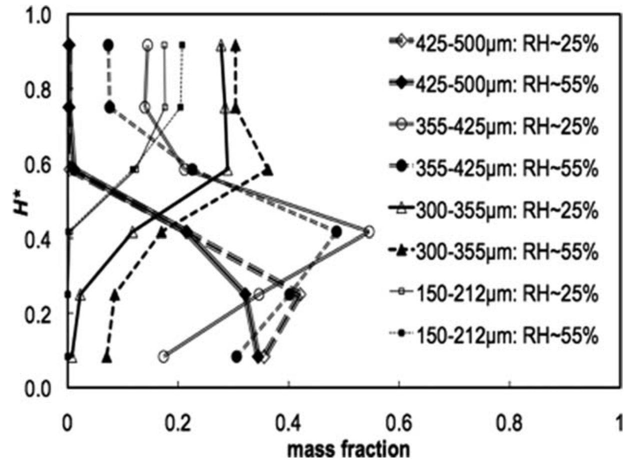

Figure 3. Axial species concentration profiles of Gaussian distribution with σ/d_{sm} = 30% at RH ~ 25% and RH ~ 55%.

reached; (5) abruptly shut off the gas feed to collapse the bed; (6) vacuum out axial sections of the bed for sieve analysis. As mentioned previously, this methodology is restricted to low-fluidization velocities in order to effectively eliminate the potential of segregation upon bed collapse.[9]

Reducing Electrostatics

During the preliminary experimental runs, some evidence of electrostatics was observed in the fluidized bed. For example, some sand particles were observed to be sticking to the inner walls of the Plexiglass column. The observation of electrostatics is not surprising, since contact charging between particles having the same chemical makeup but different sizes has been previously confirmed.[28,34] Because the focus of the current effort is on the impact of continuous PSD's on segregation behavior (rather than electrostatic effects), efforts were made to eliminate the effect of electrostatics. Hence, maintaining RH at above 40% by means of a humidifier placed at the inlet of the blower was used to reduce electrostatics.[16,28,29] At higher RH, the sticky nature of the sand particle to the inner wall of the Plexiglass column appeared to have attenuated. Although Figure 3 shows that axial concentration profiles at RH ~ 25% and RH ~ 55% were similar, implying the ineffectual role of electrostatics on the segregation profiles under examination in this work, all fluidization experiments were nonetheless carried out at RH above 40%.

Results and Discussion

Fluidization curves

As a first step, fluidization curves (ΔP vs. U_s) were generated for all distributions investigated to determine the complete fluidization velocity (U_{cf}) values and the quality of fluidization. The U_{cf} values are necessary to ensure complete fluidization of all particles in the bed when carrying out segregation experiments, while also ensuring operation at low-enough velocity ($1.2U_{cf}$) to eliminate potential segregation during bed collapse by keeping bed expansion to a minimum. Moreover, as previously pointed out, although the focus of this work is on Geldart Group B particles, Geldart Group D particles were also included in the wider lognormal distributions investigated (σ/d_{sm} = 30 to 70%) since the width of these distributions is greater than the range of diameters contained in Group B alone. Because Group D particles are known to exhibit poor fluidization quality, it was necessary to verify whether or not these bigger particles were completely fluidized in the column. For this assessment, a good test is the accurate prediction of bed weight (W) using the fluidization curves, as described later. Specifically, the weight of the particles fluidized by air was compared to the weight of particles loaded into the bed.

The fluidization curves of the narrowest and widest distributions of the Gaussian and lognormal distributions investigated are shown in Figure 4. The experimental values of U_{cf}, namely the point at which the bed pressure drop (ΔP) becomes constant with further increases in superficial gas velocity (U_s), are marked with vertical lines. As observed in Figure 4, the transition from the packed-bed region (line of nonzero slope) to the fluidized region (horizontal line) for continuous distributions is not abrupt, compared to the precipitous change (i.e., discontinuity in slope values) expected for a monodisperse distribution. Especially for the wider lognormal distributions (Figure 4c and d), the transition is a smooth elbow, due to the range of minimum fluidization velocities (U_{mf}) of the various particle sizes contained in the distribution. Accordingly, a protocol for determining U_{cf} that identifies the point of minimum U_s at which the data points are within ±1% of the W/A value was used. For all the distributions investigated, the experimental pressure drops (data points) plateau at the measured bed weight (W) divided by the cross-sectional area (A) (horizontal dashed line), indicating that the bed was completely fluidized beyond U_{cf}. As expected, U_{cf} values are similar, because the distributions are centered about the same Sauter-mean diameter (d_{sm}); it has been reported that U_{cf} values of the continuous distributions agree with U_{mf} of the mean particle size.[10,11] Notably, the U_{cf} value of the widest distribution investigation, specifically lognormal distribution with σ/d_{sm} = 70%, is slightly higher than the other distributions, presumably due to the presence of the largest amount of coarse Group D particles.

Interestingly, although a bed of monodisperse Group D particles do not fully fluidize, their presence in the lognormal distributions did not result in the underprediction of W/A. In particular, as displayed in Figure 5, "monodisperse" Group D particles of size range 1-2 mm give a 13% underprediction of W/A, indicating that the particles are not fully fluidized, and providing evidence that Group D particles exhibit poor fluidization quality. However, as previously shown in Figure 4c and d, the presence of the same Group D particles in lognormal distributions does not give rise to the underprediction of W/A, even though they represent up to 24% by mass of the lognormal distribution with σ/d_{sm} = 70%. This observation that the presence of a wide range of particle sizes enhances fluidization of larger particles is especially noteworthy since the U_{mf} of the monodisperse Group D system, which agrees with existing empirical correlations,[1] is about six times that of the continuous distributions contained in Figure 4. A possible explanation for the

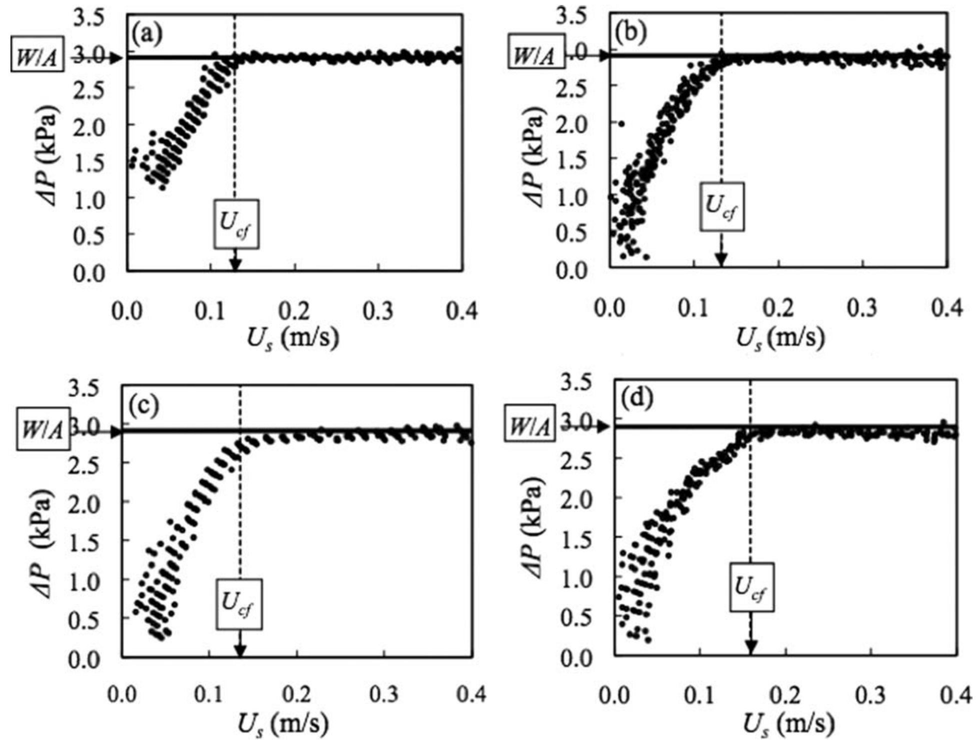

Figure 4. Fluidization curves of Gaussian distributions with (a) σ/d_{sm} = 10%, and (b) σ/d_{sm} = 30%, and lognormal distributions with (c) σ/d_{sm} = 30%, and (d) σ/d_{sm} = 70%.

The data points represent bed pressure drops during repeated defluidization and fluidization, while the horizontal dashed line represents the experimental bed weight over cross-sectional area (W/A).

improvement of fluidization has been shown via discrete element model (DEM) simulations showing that systems with wide PSD exhibited higher particle velocities around bubbles and faster bubble growth, hence, enhancing fluidization.[35] As will be further elucidated in the following section, the width of a continuous distribution is an important factor in the hydrodynamics of fluidization.

Axial Concentration Profiles

The axial concentration profiles for the Gaussian distributions investigated are shown in Figure 6. The mass-based frequency (f_m) is on the *x*-axis and represents the proportion of each sieve cut for a given axial section. The dimensionless height (H*) is on the *y*-axis. H^* is used for easier comparison across the distributions, because the different proportions of various particle sizes in different distributions result in different packing heights. A vertical line on these plots implies no axial variation of concentration for a given sieve cut, thereby indicating a perfectly mixed system, while a contoured line implies segregation of different-sized particles. At least two experiments were carried out for each distribution, and the error bars represent the experimental variations, expressed as the difference between the maximum and minimum values obtained. Since the overall mass fraction of a given sieve cut changes between distributions of different widths, the appropriate comparison of the extent of segregation between the various distributions is the verticality of the lines on the axial segregation plots, rather than the absolute values of f_m. For the distribution with $\sigma/d_{sm} = 10\%$ (Figure 6a), it is observed that the H* vs. f_m plots for the various sieve cuts are almost vertical, indicating that the system is well-mixed. On the other hand, for the distribution

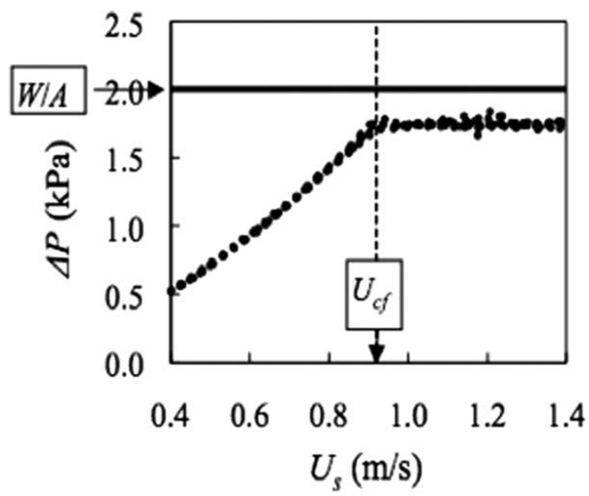

Figure 5. Fluidization curve of monodisperse Geldart Group D sand of particle-size range 1-2 mm.-

The data points represent repeated fluidization and defluidization, while the horizontal bold line represents the experimental W/A.

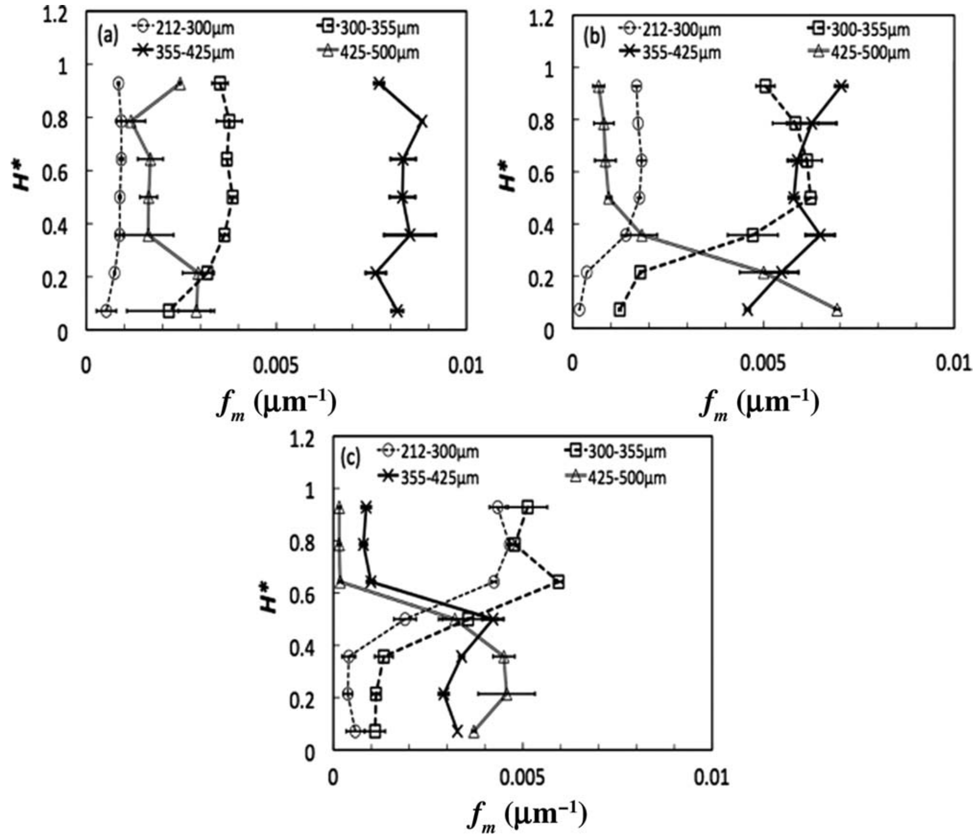

Figure 6. Axial concentration profiles of Gaussian distributions with (a) σ/d_{sm} = 10%, (b) σ/d_{sm} = 15%, and (c) σ/d_{sm} = 30%.

with $\sigma/d_{sm} = 30\%$ (Figure 6c), the plots are far from vertical, indicating that comparatively extensive segregation is observed among the different sizes of sand particles. The gradual increase in segregation as the width of distribution is increased, is, hence, apparent in Figure 6, providing experimental evidence to the DEM[21] and continuum-model[22] simulation findings that wider distributions exhibit more extensive segregation for a gas-fluidized bed for Gaussian distributions in this range of widths. Figure 6 also shows that the mass fractions of the coarser and finer particles are greater at the bottom and top of the bed, respectively, consistent with modeling and experimental[6–9] (see references and references therein) findings of binary systems of size-segregating systems.

In addition to the axial concentration plots presented, the overall extent of segregation for each starting distribution can be compared using a single integrated quantity. This measure, examples of which include the mixing index (M), and segregation index (s), has been derived for binary distributions. The mixing index (M) takes the form[36,37]

$$M = \frac{x}{\langle x \rangle} \tag{3}$$

where x is the concentration of the larger particles in the topmost layer of the particle bed, and $\langle x \rangle$ is the average concentration of the larger particles in the entire bed, such that $M = 1$ corresponds to perfect mixing and $M = 0$ implies perfect segregation. On the other hand, the segregation index (s) takes into account both particle sizes, and is expressed as[38]

$$s = \frac{S - 1}{S_{\max} - 1}. \tag{4}$$

The numerator in Eq. 4 contains the ratio of the actual heights of the small and large particles which is indicative of the actual degree of segregation

$$S = \frac{\langle h_{small} \rangle}{\langle h_{large} \rangle} \tag{5}$$

where $\langle h_{\text{small}} \rangle$ and $\langle h_{\text{large}} \rangle$ are the calculated average dimensionless heights of the small and large particles, respectively. Specifically

$$\langle h_{small} \rangle = \sum_i \left(x_{small,i} * h_i \right) \tag{6}$$

$$\langle h_{large} \rangle = \sum_i \left(x_{large,i} * h_i \right) \tag{7}$$

where h_i represents the dimensionless height (with respect to the bed height) of each axial section that is vacuumed out and analyzed for PSD, and x_i represents the mass fraction of the species in that particular axial section.

The denominator in Eq. 4 contains the associated maximum degree of segregation, which occurs when the small

Table 1. Segregation Indices (s_{cont}) of Gaussian Distributions Investigated

(%)	s_{cont}	% by mass of '*large*'	% by mass of '*small*'
10	0.024	16.8	25.9
15	0.175	21.2	12.5
30	0.284	18.9	28.7

particles are wholly in the top portion while the large particles are all in the bottom portion

$$\langle h_{small} \rangle_{max} = x_{large} + 0.5x_{small} = 1 - 0.5x_{small} \tag{8}$$

$$\langle h_{large} \rangle_{min} = 0.5x_{large} = 0.5(1 - x_{small}). \tag{9}$$

Hence, the maximum degree of segregation can be expressed as

$$S_{\max} = \frac{\langle h_{\text{small}} \rangle_{\max}}{\langle \text{h}_{\text{large}} \rangle_{\min}} = \frac{2 - x_{small}}{1 - x_{small}}. \tag{10}$$

Accordingly, the segregation index (s) is defined in Eq. 4 such that $s = 1$ corresponds to perfect segregation while $s = 0$ implies perfect mixing. Since M considers only the bigger particles and topmost layer, it is not as inclusive as s, which takes into account concentrations and averaged heights of both species in the binary mixture. Hence, we consider only s to more accurately represent our data. Nonetheless, it is observed that M shows the same trends.

In order to quantify the extent of segregation for *continuous*-size distributions, a new segregation index (s_{cont}) is introduced here based on an extension of the segregation index for binary mixtures (s). Specifically, the modifications made to s_{cont} are twofold: (1) the definitions of "*large*" and "*small*" needs to be changed, because the demarcation is not as clear-cut as in a binary distribution, and (2) Eq.10 only works for a binary distribution, and, hence, was modified as described later (Eq. 11). Regarding (1), "*large*" and "*small*" are now defined as the uppermost and lowermost sieve cuts that constitutes at least 10% by mass of the total mass of the bed, since the maximum experimental variation in the segregation data was observed to be 10% by mass. Regarding (2), the maximum extent of overall segregation is redefined for a more general case because x_{large} is no longer simply $(1-x_{\text{small}})$, as was assumed in Eqs. 8–10. By lifting this assumption, a more general form of $S_{\max}$ is obtained

$$S_{\max} = \frac{2x_{large} + x_{small}}{x_{large}}. \tag{11}$$

Similar to the binary definition, the aforementioned modification for continuous distributions ensures that $s_{\text{cont}} = 1$ corresponds to complete segregation, while $s_{\text{cont}} = 0$ implies complete mixing. These segregation indices (s_{cont}) and the corresponding makeup of "large" and "small" particles are presented in Table 1. It is worth noting that although the percentage of "large" and "small" particles are not constant through the various distributions due to limited sieve meshes available, effort was made to make the numbers similar for the fairest comparison possible. Results clearly show an increase in s_{cont}, which corresponds to an increase in the extent of segregation, with the width of the Gaussian distributions.

Analogous axial concentration profiles and segregation indices (s_{cont}) are contained in Figure 7 and Table 2 for the lognormal distributions investigated. As evident in Figure 7, while the segregation profiles for σ/d_{sm} = 10 and 70% are vertical lines indicating well-mixed systems, those for σ/d_{sm} = 30 and 50% are contoured lines indicating segregated systems. This trend is corroborated with the data contained in Table 2, which shows quantitatively that while lognormal distributions with σ/d_{sm} = 10 and 70% have similarly low values of s_{cont}, the distribution with σ/d_{sm} = 30% has the highest s_{cont}, implying the most segregated system. This nonmonotonic segregation behavior of lognormal distributions has not been previously reported in simulations or experiments. Nonetheless, nonmonotonic segregation levels have been observed in *binary* mixtures with species of *different material density* (but same size), wherein segregation has been observed to be strongest for intermediate compositions, with fairly well-mixed systems at low- or high-concentrations of jetsam.[9] Looking back at Figure 2b, it is apparent that the distribution with σ/d_{sm} = 70% does consist of the greatest amounts of the finest, as well as largest particles. However, it is worthwhile to note that previous work on binary mixtures does not reveal a nonmonotonic segregation behavior when considering species with the same material density but different sizes,[9] which is most analogous to the continuous PSD's under consideration in this work.

A possible explanation may be related to the bubbling phenomenon. Rowe et al.[36] were among the first to suggest that rising bubbles are the vehicles for particle mixing. Quantitatively, Nienow et al.[39] found the rate of bubbling, which has been associated with mixing behavior, as being proportional to the excess gas velocity (U_{excess}) defined as

$$U_{excess} = k(U_s - U_{mf,\, small}) \tag{12}$$

where k is a proportionality constant, $U_{mf,\text{small}}$ is the minimum fluidization velocity of the smallest particles, and U_s is the operating superficial gas velocity (which in this work is $1.2U_{cf}$). When U_{excess} is large, mixing predominates; and when U_{excess} is small, segregation takes over. The slightly larger U_{cf} of the lognormal distribution with σ/d_{sm} = 70% (Figure 4d) may, thus, be associated with more mixing: while a wider distribution is expected to result in more segregation by virtue of the increased number of species present, the effect of mixing based on excess gas velocity (U_{excess}) may tilt the mixing-segregation balance the other way. Subsequently, previous studies have shown that a wide-size distribution usually give the highest reactor efficiency, while the narrow blend give the lowest,[10] possibly associated with bubbling patterns in bed.[40] DEM simulations[35] have shown that systems with a wide PSD exhibit higher particle velocities around bubbles, while experiments[13,14] corroborated the enhancement of mixing through producing smaller and faster-moving bubbles. However, it can be argued that if the lognormal distribution with σ/d_{sm} = 70% exhibits the least extent of segregation due to its greatest width, why is it that the Gaussian distribution with the greatest width of σ/d_{sm} = 30% did not similarly exhibit a well-mixed system? Grace and

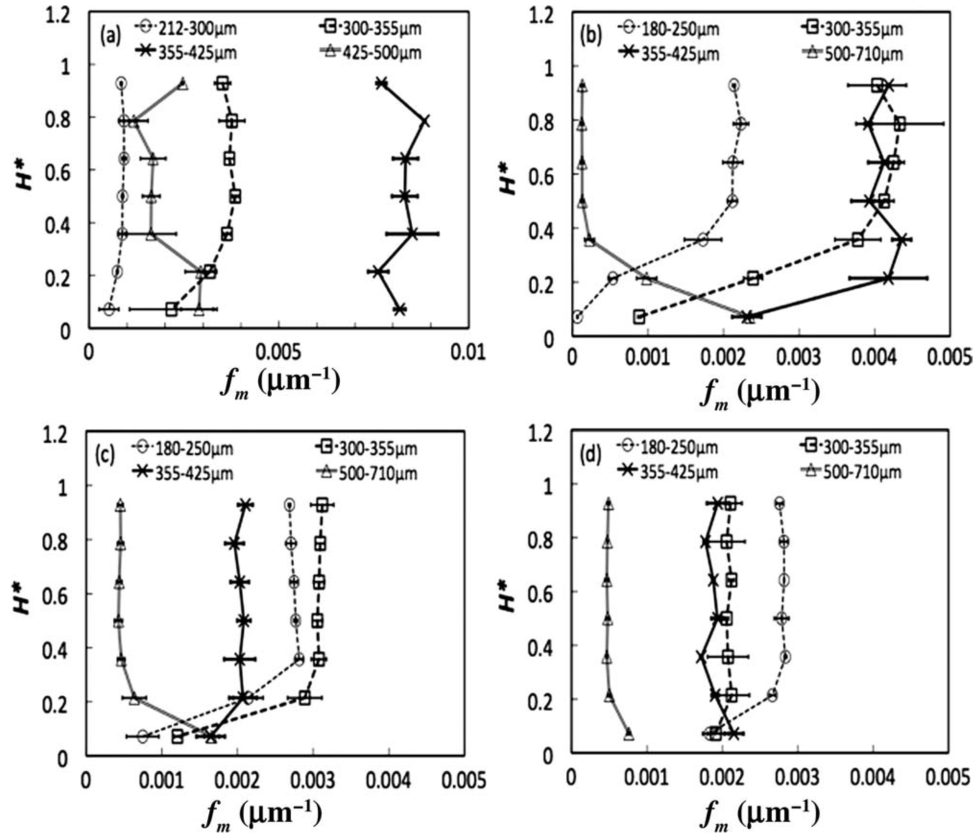

Figure 7. Axial segregation profiles of lognormal distributions with (a) σ/d_{sm} = 10%, (b) σ/d_{sm} = 30%, (c) σ/d_{sm} = 50%, and (d) σ/d_{sm} = 70%.

Sun[14] reviewed the influence of PSD on fluidized-bed reactors and asserted that fines content *per se* is not a sufficient parameter to characterize segregation; their nature and the overall size distribution have to be considered. Nonetheless, more work is needed to get a clearer physical picture of the mechanisms leading to the nonmonotonic segregation patterns observed here.

The segregation extents for the various widths of Gaussian and lognormal distributions investigated (Tables 1 and 2) are compared directly in the plot of segregation indices (s_{cont}) as in Figure 8. As pointed out previously, results in this work suggest that, while the segregation extents are positively correlated with the PSD widths for Gaussian distributions, a nonmonotonic behavior exists for lognormal distributions. Comparing the segregation indices (s_{cont}) shows that the lognormal distribution with $\sigma/d_{sm} = 50\%$ is less segregated that the Gaussian distribution with $\sigma/d_{sm} = 30\%$. At first glance, this observation seems contrary to previous simulation work for fluidized beds,[21,22] which compared segregation in Gaussian distributions of σ/d_{sm} up to 30%, and a lognormal distribution of $\sigma/d_{sm} = 50\%$, and reported that the lognormal distribution exhibits the most extensive segregation. However, two distinctions between the previous simulations[21]

Table 2. Segregation Indices (s_{cont}) of Lognormal Distributions Investigated

(%)	s_{cont}	% by mass of '*large*'	% by mass of '*small*'
10	0.024	16.8	25.9
30	0.168	13.2	13.6
50	0.074	18.1	27.6
70	0.022	19.7	19.6

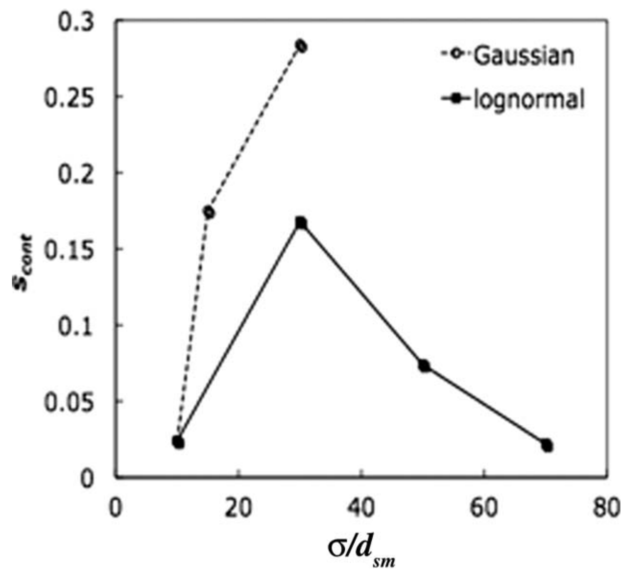

Figure 8. Plot showing the correlation between s_{cont} and σ/d_{sm} for Gaussian and lognormal distributions.

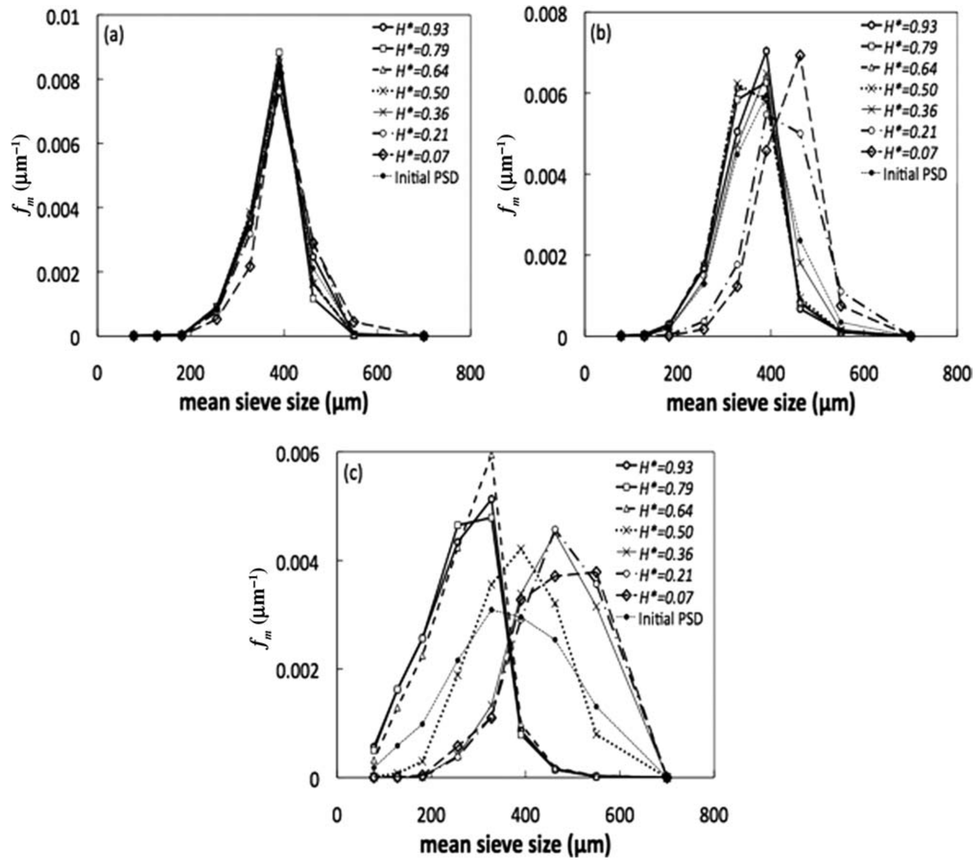

Figure 9. Axial PSD's of Gaussian distributions with (a) σ/d_{sm} = 10%, (b) σ/d_{sm} = 15%, and (c) σ/d_{sm} = 30%.

and the current experimental work are worth pointing out. First, the PSD's in the simulations were number-based, whereas the PSD's in the current work are mass-based. Perhaps more importantly, however, is a difference in particle properties. In comparing distributions of different widths, the previous simulation work[21] also incorporated a change in the restitution and friction coefficients of the particles. More specifically, the widest lognormal distribution investigated ($\sigma/d_{rms} = 50\%$, where d_{rms} is the root-mean-square diameter) also had the least dissipative particles, which led to a bubble-less (and thus relatively segregated) system; the narrower distributions investigated in the simulations had more dissipative particles and correspondingly exhibited bubbling (see Hoomans et al.[18] for further discussion of relationship between particle properties and bubbling characteristics). In the current see of experiments, the same material (sand) was consistently used, and bubbles were observed in all systems. Hence, a strict comparison between the previous simulations[21] and current experiments is not warranted.

Shape of local PSD

In addition to the axial concentration profiles associated with each size range given previously, the shape of the size distribution (Gaussian or lognormal) at a given axial height is also of interest. Although the PSD of the entire bed mass is specified (e.g., Gaussian with $\sigma/d_{sm} = 10\%$), segregation of particles may lead to different *local* PSD's. For the Gaussian distributions investigated, Figure 9 shows how the shapes of the local PSD's vary axially along the bed. The local PSD's are nearly superimposed for the distribution with $\sigma/d_{sm} = 10\%$ (Figure 9a), except for a slight rightward shift of the PSD at the bottommost axial section. This behavior further indicates a well-mixed system, as previously elucidated, implying that a system with a narrow distribution behaves similar to a monodisperse system. For the distributions with $\sigma/d_{sm} = 15$ and 30% (Figure 9b and c), the PSD's associated with various axial locations are more separated, with a rightward shift of the PSD's as the particle bed is traversed downward, indicating again the segregation of bigger particles toward the bottom. Furthermore, for the distribution with $\sigma/d_{sm} = 10\%$ (Figure 9a), and 15% (Figure 9b), the PSD's at each axial location still resemble a Gaussian distribution. However, more deviations are observed for the distribution with $\sigma/d_{sm} = 30\%$ (Figure 9c), especially for the two bottom-most PSD's.

To better quantify how closely the shape of the local distribution mimics that of the overall distribution, comparisons between the (local) experimental PSD and an exact Gaussian PSD (as given by Equation 1) are made by minimizing the root-mean-square (rms) difference between them via changing the values of d_{sm} and σ/d_{sm}. It should be noted that the local distributions may have different d_{sm} and σ/d_{sm}, but still characterized by the same shape (i.e., Gaussian or lognormal). For the Gaussian distribution with $\sigma/d_{sm} = 10\%$, the statistics of the PSD's show that the d_{sm} and σ/d_{sm} for the

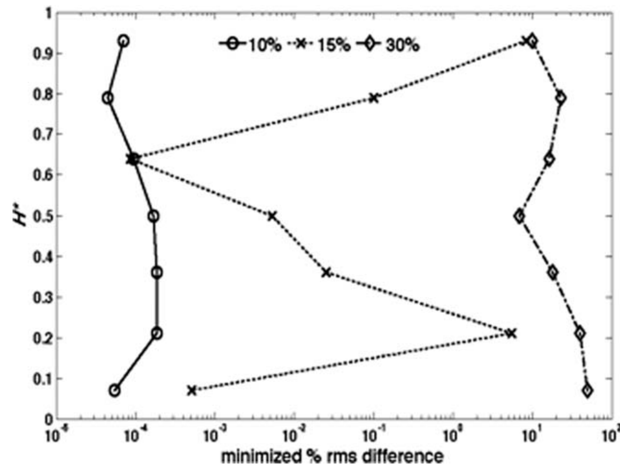

Figure 10. Plot showing variation of the minimized rms difference between the PSD at each axial location and the equation-generated PSD for the Gaussian distributions investigated.

PSD at each axial location are similar to the initial PSD with d_{sm}'s approximating 375μm and σ/d_{sm}'s approximating 10%, further indicating a well-mixed system. Axial variations in minimized rms differences between experimentally generated and exact PSD's for each Gaussian distribution are plotted in Figure 10. As shown in Figure 10, the rms differences are less than 0.001 and 10% for all local PSD's obtained for the Gaussian distributions with σ/d_{sm} of 10 and 15%, respectively. On the other hand, rms differences average about 15% for the upper few PSD's of the Gaussian distribution with σ/d_{sm} of 30%, with rms differences as high as 40% for the two bottommost PSD's. It seems that the wider the distribution, the larger the deviation of the local shape of the local PSD from an exact Gaussian, which is not surprising considering the increase in the number of species present in a wider distribution. Nonetheless, it can be concluded that the Gaussian shape of the PSD's at each axial section of the bed is largely preserved, which agrees with previous simulation findings in both granular and gas-fluidized systems.[21,23] The observation that the bottommost PSD's no longer remain Gaussian has also been shown in DEM simulations,[21] and it was postulated to be due to the bottom regions being more stagnant.

For lognormal distributions, the analogous plots for variations in the local PSD are shown in Figures 11 and 12. Figure 11 again shows that the shape of the local PSD at each axial location resembles the shape of the *overall* PSD, namely a lognormal distribution. Figure 12 further quantifies how similar each local PSD is to an exact lognormal PSD by a plot of the axial variation of the minimized rms difference between the experimentally obtained and exact lognormal PSD. The increased discrepancies for wider lognormal

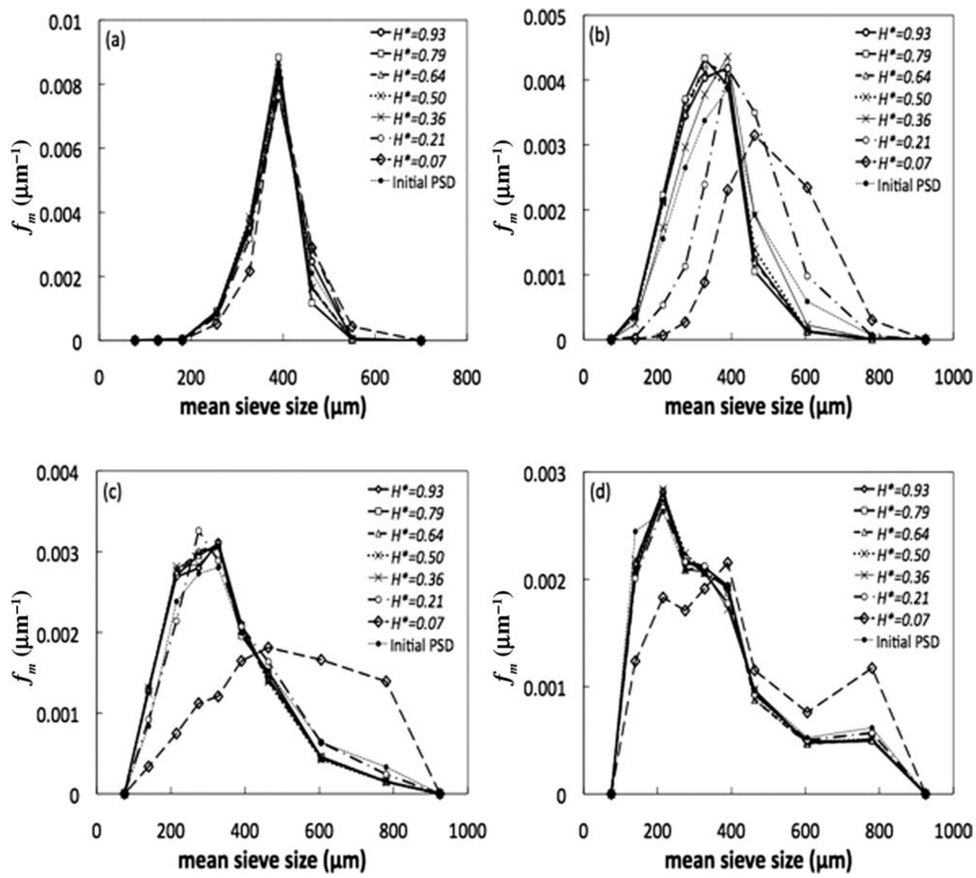

Figure 11. Axial PSD's for the lognormal distributions with (a) σ/d_{sm} = 10%, (b) σ/d_{sm} = 30%, (c) σ/d_{sm} = 50%, and (d) σ/d_{sm} = 70%.

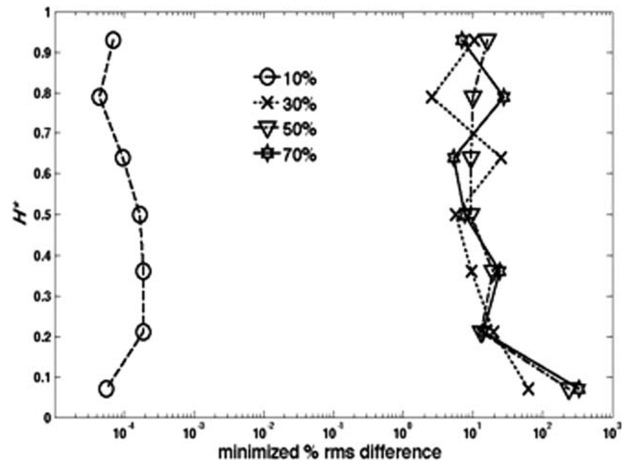

Figure 12. Plot showing variation the minimized rms difference between the PSD at each axial location and the equation-generated PSD for the lognormal distributions investigated.

distributions of $\sigma/d_{sm} \geq 30\%$ are much greater than that for $\sigma/d_{sm} = 10\%$. Also, it is apparent that the greatest discrepancy for lognormal distributions with $\sigma/d_{sm} > 30\%$ is of the bottommost PSD at $H^* = 0.07$. Similar to the findings for the Gaussian distribution with $\sigma/d_{sm} = 30\%$, the minimized rms differences between experimentally obtained and exact PSD's for the lognormal distribution are mostly about 10%, except for the PSD's at the bottommost positions. Except for the lognormal distribution with $\sigma/d_{sm} = 10\%$, it appears that the bottommost ($H^* = 0.07$) PSD's of all the other distributions are not lognormal, presumably due to the predominance of the coarser Group D particles in the bottommost layer of the bed. As previously mentioned, DEM simulation of gas-fluidized bed has shown similarly that the measured local PSD are not Gaussian or lognormal in regions where particles move infrequently (e.g., nearly stagnant regions of the bed near the bottom).[21]

Summary

Experiments involving low-velocity, bubbling, gas-fluidized beds have been carried out for Geldart Group B particles of various widths of Gaussian and lognormal (mass-based) distributions, with a focus on the axial concentration profiles. Specifically, fluidization curves were first generated to determine the velocity for complete fluidization (U_{cf}), followed by steady-state fluidization at $1.2U_{cf}$. Although only Group B particles were used in the Gaussian distributions, up to 24% by mass of the widest lognormal distribution ($\sigma/d_{sm} = 70\%$) was made up of Group D particles. Due to the nature of the lognormal distribution, it is not possible to restrict all particle sizes to within Group B classification, and larger Group D particles have to be included for an accurate representation.

The complete fluidization velocity (U_{cf}) is the minimum superficial gas velocity (U_s) beyond which bed pressure drop (ΔP) equals to W/A. As such, W/A is a good indicator for quality of fluidization. Interestingly, although monodisperse Geldart Group D particles exhibited poor fluidization, as indicated by the failure of the bed pressure drop to attain W/A, their presence in the wider lognormal distributions did not stunt the quality of fluidization.

Results for the Gaussian ($\sigma/d_{sm} = 10\%$, 15%, and 30%), and lognormal ($\sigma/d_{sm} = 10\%$, 30%, 50%, and 70%) distributions investigated show that (1) increased segregation is observed for wider Gaussian distributions, whereas a nonmonotonic correlation exist between segregation extents and width of lognormal distributions, (2) similar to previous findings for binary mixtures, finer and coarser particles tend to segregate, respectively to the top and bottom, and (3) the shape of the PSD (i.e., Gaussian or lognormal) at each axial section is preserved with respect to the overall PSD, except for the bottommost PSD's of the wider distributions. With the exception of the surprising finding of the nonmonotonic behavior of the segregation extents with increasing widths of lognormal distributions, the experimental findings agree with previous discrete particle simulations[21] and continuum modeling[22] of gas-solid fluidized beds with continuous-size distributions. It should be noted that the nonmonotonic segregation behavior with respect to width of the lognormal distributions is not necessarily at odds with previous simulation[21] results. More specifically, bubbles were absent in the simulation of the widest lognormal distribution[21], presumably due to a change in particle properties (restitution and friction coefficients), whereas bubbles were consistently observed in the current experiments, which all involved the same particle material (sand). More work is needed to resolve this issue definitively.

An interesting follow-up of this work is the investigation of bubbling phenomena associated with the various widths of the Gaussian and lognormal PSD's in order to see if there is a link between the bubbling and segregation behaviors. Bubbles have been reported to be mixing agents, and may hold the key to developing a clearer physical picture to explain the nonmonotonic segregation behavior with respect to the widths of the lognormal distributions. For example, DEM simulations have indicated that systems with a wide particle-size distribution exhibit higher particle velocities around bubbles, resulting in faster bubble growth and its subsequent rise through the fluidized bed, thereby promoting mixing.[35] Experimental evidence of this observation would be useful, because bubbling pattern and segregation behavior are expected to be tightly coupled.

Finally, the results of this work are expected to find additional value in the validation of two-fluid models for continuous-size distributions. To date, the vast majority of two-fluid modeling efforts have focused on binary mixtures. The ability to adapt the various closures (kinetic theory, drag laws, etc.) to continuous distributions remains largely untested, partially due to the previous lack of detailed experimental data.

Acknowledgments

The authors gratefully acknowledge funding from the Dept. of Energy (DE-FC26-07NT43098), and the National Science Foundation (CBET-0318999).

Literature Cited

1. Kunii D, Levenspiel O. *Fluidization Engineering*. Massachusetts: Butterworth-Heinemann; 1991.

2. Fan LS, Zhu C. *Principles of Gas-Solid Flows*. New York: Cambridge University Press; 1998.
3. Yang W. *Handbook of Fluidization and Fluid-Particle Systems*. New York: Marcel Dekker, Inc.; 2003.
4. Merrow EW. Estimating startup times for solids-processing plants. *Chem Eng*. 1988;95(15):89–92.
5. Merrow EW. Linking R-and-D to problems experienced in solids processing. *Chem Eng Prog*. 1985;81(5):14–22.
6. Rowe PN, Nienow AW. Particle mixing and segregation in gas-fluidized beds - review. *Powder Technol*. 1976;15(2):141–147.
7. Tang P, Puri VM. Methods for minimizing segregation: A review. *Part Sci Technol*. 2004;22(4):321–337.
8. Cui HP, Grace JR. Fluidization of biomass particles: A review of experimental multiphase flow aspects. *Chem Eng Sci*. 2007;62(1–2):45–55.
9. Joseph GG, Leboreiro J, Hrenya CM, Stevens AR. Experimental segregation profiles in bubbling gas-fluidized beds. *AIChE J*. 2007; 53(11):2804–2813.
10. Sun GG, Grace JR. The effect of particle-size distribution on the performance of a catalytic fluidized-bed reactor. *Chem Eng Sci*. 1990;45(8):2187–2194.
11. Gauthier D, Zerguerras S, Flamant G. Influence of the particle size distribution of powders on the velocities of minimum and complete fluidization. *Chem Eng J*. 1999;74(3):181–196.
12. Lin CL, Wey MY, You SD. The effect of particle size distribution on minimum fluidization velocity at high temperature. *Powder Technol*. 2002;126(3):297–301.
13. Beetstra R, Nijenhuis J, Ellis N, van Ommen JR. The influence of the particle size distribution on fluidized bed hydrodynamics using high-throughput experimentation. *AIChE J*. 2009;55(8):2013–2023.
14. Grace JR, Sun G. Influence of particle-size distribution on the performance of fluidized-bed reactors. *Can J Chem Eng*. 1991;69(5): 1126–1134.
15. Sun G, Grace JR. Experimental-determination of particle dispersion in voids in a fluidized-bed. *Powder Technol*. 1994;80(1):29–34.
16. Hoffmann AC, Romp EJ. Segregation in a fluidized powder of a continuous size distribution. *Powder Technol*. 1991;66(2):119–126.
17. Lin CL, Wey MY. Statistical and power spectral analysis of quality of fluidization for different particle size distributions at high temperature. *Adv Powder Technol*. 2004;15(1):79–96.
18. Hoomans BPB, Kuipers JAM, van Swaaij WPM. Granular dynamics simulation of segregation phenomena in bubbling gas-fluidised beds. *Powder Technol*. 2000;109(1-3):41–48.
19. Bokkers GA, Annaland MVS, Kuipers JAM. Mixing and segregation in a bidisperse gas-solid fluidised bed: a numerical and experimental study. *Powder Technol*. 2004;140(3):176–186.
20. van Wachem BGM, Schouten JC, van den Bleek CM, Krishna R, Sinclair JL. CFD modeling of gas-fluidized beds with a bimodal particle mixture. *AIChE J*. 2001;47(6):1292–1302.
21. Dahl SR, Hrenya CM. Size segregation in gas-solid fluidized beds with continuous size distributions. *Chem Eng Sci*. 2005;60(23): 6658–6673.
22. Fan R, Fox RO. Segregation in polydisperse fluidized beds: Validation of a multi-fluid model. *Chem Eng Sci*. 2008;63(1):272–285.
23. Dahl SR, Hrenya CM. Size segregation in rapid, granular flows with continuous size distributions. *Phys Fluids*. 2004;16(1):1–13.
24. Beetstra R, van der Hoef MA, Kuipers JAM. Numerical study of segregation using a new drag force correlation for polydisperse systems derived from lattice-Boltzmann simulations. *Chem Eng Sci*. 2007;62(1-2):246–255.
25. Leboreiro J, Joseph GG, Hrenya CM, Snider DM, Banejee SS, Galvin JE. The influence of binary drag laws on simulations of species segregation in gas-fluidized beds. *Powder Technol*. 2008;184(3):275–290.
26. Van der Hoef MA, Beetstra R, Kuipers JAM. Lattice-Boltzmann simulations of low-Reynolds-number flow past mono- and bidisperse arrays of spheres: results for the permeability and drag force. *J Fluid Mech*. 2005;528:233–254.
27. Yin XL, Sundaresan S. Drag law for bidisperse gas-solid suspensions containing equally sized spheres. *Ind Eng Chem Res*. 2009;48(1):227–241.
28. Hendrickson G. Electrostatics and gas phase fluidized bed polymerization reactor wall sheeting. *Chem Eng Sci*. 2006;61(4):1041–1064.
29. Guardiola J, Rojo V, Ramos G. Influence of particle size, fluidization velocity and relative humidity on fluidized bed electrostatics. *J Electrostat*. 1996;37(1-2):1–20.
30. Ciborowski J, Wlodarski A. On electrostatic effects in fluidized beds. *Chem Eng Sci*. 1962;17(1):23–32.
31. Tardos G, Pfeffer R. A method to measure electrostatic charge on a granule in a fluidized-bed. *Chem Eng Commun*. 1980;4(6):665–671.
32. Geldart D. Types of gas fluidization. *Powder Technol*. 1973;7(5): 285–292.
33. Hinds WC. *Aerosol technology: Properties, Behavior, and Measurement of Airborne Particles*. 2nd ed. New York: Wiley; 1999.
34. Zhao HL, Castle GSP, Inculet II, Bailey AG. Bipolar charging of poly-disperse polymer powders in fluidized beds. *IEEE Trans Ind Appl*. 2003;39(3):612–618.
35. Tagami N, Mujumdar A, Horio M. DEM simulation of polydisperse systems of particles in a fluidized bed. *Particuology*. 2009;7(1):9–18.
36. Rowe PN, Partridge BA, Ardran GM, Lyall E. Bubbles in fluidized beds. *Nature*. 1962;195(4838):278–279.
37. Wu SY, Baeyens J. Segregation by size difference in gas fluidized beds. *Powder Technol*. 1998;98(2):139–150.
38. Goldschmidt MJV, Link JM, Mellema S, Kuipers JAM. Digital image analysis measurements of bed expansion and segregation dynamics in dense gas-fluidised beds. *Powder Technol*. 2003;138(2-3):135–159.
39. Nienow AW, Rowe PN, Cheung LYL. Quantitative-analysis of mixing of 2 segregating powders of different density in a gas-fluidized bed. *Powder Technol*. 1978;20(1):89–97.
40. Zenz F, Othmer D. *Fluidization and Fluid-Particle Systems*. New York: Reinhold Publishing Corp; 1960:278.

Manuscript received Sept. 20, 2009, revision received Dec. 11, 2009, and final revision received Feb. 16, 2010.